THE JOURNAL OF PHYSICAL CHEMISTRY B

Article

pubs.acs.org/JPCB

Electric Field as a Disaggregating Agent for Amyloid Fibrils

Andrij Baumketner*

Institute for Condensed Matter Physics, National Academy of Sciences of Ukraine, 1 Svientsistsky Str, Lviv 79011, Ukraine

ABSTRACT: Folding and aggregation lie on competing reaction pathways in proteins. Altering the occupancy of one pathway is automatically relayed to the other pathway, leading to a shift in the balance between the two processes. In particular, it is known that the stabilization of the native state through mutations or solvent alterations is able to halt aggregation. In this work, we explore the feasibility of using external electric field as an agent preventing aggregation through the promotion of folding. We use an atomically accurate protein model and computer simulations to investigate folding and aggregation of alanine polypeptides in electric field of varying strength. The studied peptides are mostly unstructured in the absence of the field but experience a transition into α-helical states when the field is applied. The transition is accompanied by the disassembly of preseeded stacked β-sheets, which are used as a model of amyloid fibrils, suggesting that electric field can be employed to control aggregation propensity of intrinsically disordered peptides. According to our calculations, the strength of the field required for the disaggregation could be suitable for both controlled *in vitro* experiments as well as for experiments on live cells. Additionally, our estimates suggest that endogenous electric fields may have a significant effect on *in vivo* amyloid formation.

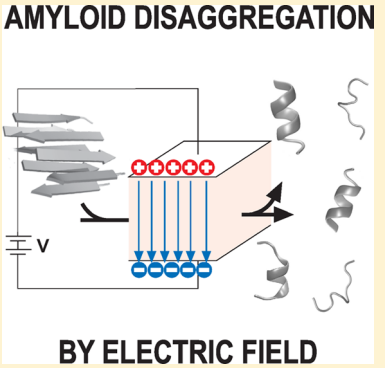

INTRODUCTION

Amyloid *fibrils* are macromolecular filaments of nanometer dimensions that are formed as a result of protein aggregation.[1] Rich in β-structure, amyloid fibrils have well-defined and specific biological functions in nature;[2,3] however, they are best known for their involvement in a host of neurodegenerative diseases.[1] While the exact cause of these diseases remains unclear, disaggregating amyloid fibrils has emerged as one of the most important therapeutic strategies.[4−6] Because of their highly ordered structure, amyloid fibrils have also become a new and promising material in nanotechnology.[7] The ability to control amyloid formation is, therefore, important from both medical as well as technological perspectives.

Aggregation and folding are intricately connected.[8] While the exact relationship between the two processes remains the subject of a vigorous debate,[9−12] it has been firmly established that proteins need to unfold before they can form amyloid.[13−18] Unfolding increases the population of disordered or partially folded states[11] which, unlike the native state, are compatible with the structure of amyloid. Partitioning into folding and aggregation pathways is controlled by nonoverlapping stretches of residues in the protein primary structure.[19] If destabilization of the native state enhances aggregation[17,18] then stabilization is expected to have the opposite effect. Indeed, making the native state more stable globally, through favorable mutations[17] or through ligand binding,[20,21] is seen to suppress amyloid formation. Similarly, mutations that promote structure locally are also able to reduce the propensity for aggregation.[22] The exact effect that the stability of the native state has on the aggregation pathways may depend on the nature of the studied protein. In proteins whose fibril assembly relies on on-path helical intermediates, for instance, enhanced folding accelerates aggregation instead of slowing it down.[23] In general, however, stabilization is expected to cause fibril disaggregation, since the native conformations are not compatible with the structure of fibrils. Previously, enhanced folding has been suggested as a tool to prevent amyloid formation.[20,22]

In this paper, we present calculations exploring the use of electric field as an agent able to disaggregate amyloid fibrils through the stabilization of the folded helical conformations. The effect of external electric field on biological molecules has been studied extensively for over more than 5 decades.[24−26] These studies have led to two prominent mechanisms of molecule-field interactions. First, it is alignment of macromolecules with permanent or induced dipoles along the axis of the applied field. In support of this mechanism, permanent dipole moments were measured for short DNA sequences[27] and proteins,[28] enabling the observation of preferential orientation in the external field. Second, it was suggested that conformational transitions may occur due to the direct interaction of the molecular dipoles with the field. This mechanism is based on a simple argument that conformations with larger dipole moments gain more in statistical weight from interactions with the field than do the states with the lower moments. The expected result is a shift of population, driven by the field, toward the states with the largest moments. Despite its simplicity, this scenario remained controversial for some time. The first evidence of the direct field effect dates back to the work of Schwarz and Seelig,[29] who interpreted the results of their dielectric dispersion measurements for a synthetic peptide based on glutamic acid as indicating a coil-to-helix transition. The kinetics theory developed by Schwarz[30] for helix transition

Received: September 11, 2014
Revised: November 26, 2014

   dx.doi.org/10.1021/jp509213f | *J. Phys. Chem. B* XXXX, XXX, XXX−XXX

was employed to explain the observations. Measurements that led to similar conclusions were later reported by a different group for a different peptide (a derivative of aspartate).[31] But their interpretation in terms of conformational transition was questioned by Marchal,[32] who argued that the orientational effects alone could explain the observed spectrum. However, more recent studies by a number of groups and experimental techniques provide a renewed support for the direct interaction mechanism. Electric pulse experiments of Sano and Yasunaga[33] unambiguously assigned a relaxation process observed for glutamic acid–based peptides to a conformational transition. Electric birefringence experiments of Porchke[34] reported the first instance of protein unfolding by electric field. Unfolding was also detected in capillary electrophoresis experiments of an unrelated protein.[35] In sum, experimental evidence gathered so far clearly demonstrates conformational transitions under the effect of electric field. In the study of membrane proteins, this phenomenon is known as electro-conformational coupling.[36] In the theory of protein folding, the stabilizing effect of helix–dipole interactions on the native state has also been noted.[37]

We employ in this study a model alanine polypeptide that remains mostly disordered in isolation but forms fibrils in peptide solution.[38] Using a replica-exchange algorithm, we first investigate folding of the peptide in static external field and show that the field can induce transition into α-helical state. Full thermodynamic analysis is carried out for the observed transition. Next, preassembled β-sheets formed by the peptide in equilibrium are studied as a function of the field. Our simulations show that the induced folding leads to β-sheet dissociation. The results obtained for the test peptide are then extrapolated to natively unfolded peptides of arbitrary length N in order to gain insight into their behavior. On the basis of this extrapolation, we conclude that the disaggregating potency of electric field increases with growing N. For $N = 30$ and greater, the field required for triggering amyloid dissociation appears to approach the biologically relevant limit.

Taken together, our results suggest that (a) an electric field can be used as a tool to control aggregation of disordered peptides *in vitro*, perhaps in experiments on live cell cultures, and (b) endogenous fields may have a non-negligible effect on folding and aggregation of proteins, especially in the context of the integral membrane proteins.

METHODS

We use the RAPID[38] model to conduct the simulations of all systems reported in this work. The peptides are modeled in atomic detail by the OPLS/AA force field,[39] supplemented by the M6/5 set of effective potentials derived for the alanine side chains.[38] Neutralizing acetyl (ACE) and amine (NH_2) protective groups are added at the amino and carboxy termini, respectively. We use the replica-exchange protocol[40] and simulation parameters as in the original publication.[38] Additionally, electric component $\vec{F} = q_i\vec{E}$ was added to the total force acting on each charge q_i, where $\vec{E}$ is the vector of the external field. Accordingly, the total Hamiltonian was augmented with the term $H_e = -\vec{d}\vec{E}$, where $\vec{d} = \sum_i q_i\vec{r}_i$ is the dipole moment of a peptide conformation and the summation runs over all charges. The simulations were performed by GROMACS[41,42] molecular modeling package, appropriately modified. The time step was set to 2 fs. The radius of gyration R_g reported in this work was computed over the positions of C_α atoms. To avoid artifacts from periodic boundary conditions in simulations of monomers, the size of the simulation cell was chosen lagre enough to eliminate interactions among periodic images. In multichain simulations, the size of the box was set to achieve a desired peptide concentration. The summary of all simulations is shown in Table 1.

Table 1. Summary of the Simulations Conducted in this Work

simulation	simulation time (ns)	temperatures (K)	number of replicas	size of the simulation box (nm)
alanine peptide with $N = 6$; all field strengths	400	260–500	12	4.55
peptide with $N = 14$	100	260–500	12	7
peptide with $N = 50$	100	260–500	36	20.9
8 chains of hexapeptide; all field strengths.	100	260–500	24	15; 7

RESULTS

Electric Field Induces Dipole Moments in a State-Specific Manner. We consider several polyalanine peptides and provide the first systematic microscopic study of the field-driven conformational transition to date. We begin with the peptide that was studied in our previous work[38] and that contains six amino acid residues, $N = 6$. In support of its role as a model intrinsically disordered system, the studied peptide remains mostly random coil with a small population of α-helical structure[38] in the absence of the field. For simplicity, we direct the field along the X axis and use the following notations throughout the rest of the paper: $E = E_x$ for the electric field and $d = d_x$ for dipole moments.

The key to the direct interaction mechanism is the ability of the peptide to respond to electric field in a state-specific way. In the absence of the field, all orientations of the peptide are equally probable. As a result, there is no measurable dipole moment even though some conformations may carry nonzero dipoles. When the field is switched on, the symmetry of the Hamiltonian is broken and the conformations develop dipole component in the direction of the field. The resulting polarization is specific to each conformation and depends on its permanent dipole. Figure 1 shows dipole moments as a function of the strength of the field E, computed for the folded,

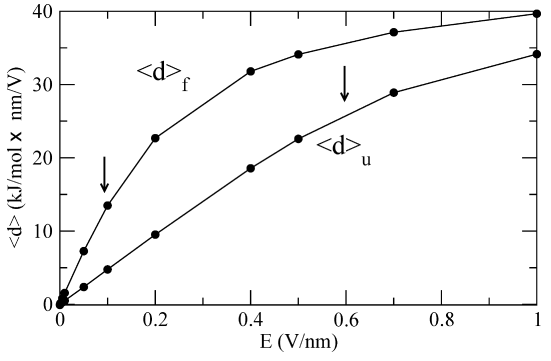

Figure 1. Dipole moments computed separately for the folded, $\langle d\rangle_f$, and unfolded, $\langle d\rangle_u$, states as a function of the strength of the field E. Clear linear regimes are seen, indicated by arrows, followed by saturation.

dx.doi.org/10.1021/jp509213f | J. Phys. Chem. B XXXX, XXX, XXX–XXX

$\langle d\rangle_f$ and unfolded, $\langle d\rangle_u$ states separately. The angular brackets indicate that the dipole moments correspond to thermodynamic equilibrium and are computed as averages. Conformations with random mean-square deviation over C_α atoms (RMSD) less than 0.1 nm from the helical state (identified as the most populated cluster) were assumed to be folded while all others were treated as unfolded. The used cutoff value was determined as the position of the first minimum in the corresponding RMSD distribution function. The data are reported for T=293 K, which is close to the temperature of 300 K for which the model was derived.[38] Both curves in Figure 1 exhibit the same qualitative behavior: the dependences are linear for small E and become saturated for stronger fields. The linear regime for the folded state applies for E < 0.1 V/nm while for the unfolded state it is limited by E = 0.6 V/nm. As the helical conformations carry a larger dipole, it is expected that the observed dipole moment is larger for the native state. But the nonvanishing magnitude of $\langle d\rangle_u$ is somewhat surprising. The side chains of polyalanine peptide studied here carry no electrical charges. In addition, the charged groups at the terminals are neutralized, as discussed in the Methods. This leaves the peptide bond as the only source of dipole moment for a given peptide conformation. If the unfolded state is assumed to be disordered, the peptide bonds in unfolded conformations should have random directions and thus produce negligible total dipole moment. The data in Figure 1 show that this assumption is not correct for the studied peptide and some residual structure remains in the unfolded state. In general, the amount of that structure is expected to depend strongly on the nature of the studied system.

Electric Field Induces Folding Into α-helical State Driven by a Combination of Enthalpic and Entropic Contributions. The effect of the electric field on conformational state a can be assessed through the thermodynamic integration:

$$\Delta F_a(E) = F_a(E) - F_a(0) = -\int_0^E \langle d\rangle_a(E)\,\mathrm{d}E \tag{1}$$

where $\Delta F_a(E) = -kT\log(Z_a(E)/Z_a(0))$ is the free energy and $Z_a(E) = \int_{\Omega_a} e^{-\beta(H-dE)}\,\mathrm{d}\Gamma$ is the configuration integral at field E associated with the state a. Here, k is the Boltzmann constant, T is the temperature, $\beta = 1/kT$, H is the Hamiltonian of the system, Ω_a defines the boundaries of state a and integration is carried out in the configuration space Γ. The symbol $\langle\cdots\rangle_a$ indicates averaging over conformations of state a. Applying the integration separately to folded and unfolded states, one can obtain the following expression for the relative free energy:

$$\Delta\Delta F(E) = \Delta F_f(E) - \Delta F_u(E) = -\int_0^E [\langle d\rangle_f - \langle d\rangle_u](E)\,\mathrm{d}E$$
$$= -kT\log\left(\frac{Z_f(E)Z_u(0)}{Z_u(E)Z_f(0)}\right) = -kT\log\left(\frac{P_f}{1-P_f}\right) - \Delta F_0 \tag{2}$$

where P_f is the occupancy of the native state at field strength E and ΔF_0 is the free energy difference between the folded and unfolded states in the absence of the field. Figure 2 shows $\Delta\Delta F$ computed in our simulations as a function of E. The errors shown in this Figure were estimated using block analysis[43] by splitting the original 400 ns trajectory into 10 pieces each 40 ns long. As the estimated autocorrelation time is less than 1 ns, the splitting produces 10 statistically independent measurements.

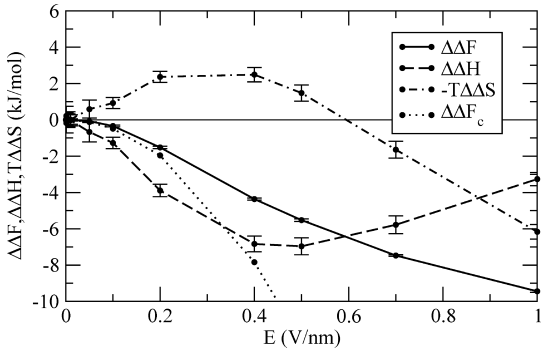

Figure 2. Field contributions to various relative thermodynamic functions of the folded and unfolded states. All field strengths enhance the folded state. The precise reasons for the stabilization vary with E as discussed in the main text. Quadratic approximation to $\Delta\Delta F$ is denoted $\Delta\Delta F_c$. Errors were estimated from block analysis by splitting the original trajectory into 10 statistically independent pieces.

On the scale of the figure, the error bars are comparable in size to the employed symbols, demonstrating good convergence of the presented data. All field strengths are seen to enhance the native helical state. The stabilization is not significant for small E < 0.2 V/nm, where $\Delta\Delta F$ is not exceeding 2 kJ/mol. For larger E, the free energy difference becomes appreciable, reaching 9 kJ/mol for E = 1 V/nm.

To determine the thermodynamic reasons why the stabilization of the native state takes place, $\Delta\Delta F$ was decomposed into entalphic and entropic contributions according to the formula

$$\Delta\Delta F(E) = \Delta\Delta H(E) - T\Delta\Delta S(E) \tag{3}$$

where both $\Delta\Delta H(E)$ and $\Delta\Delta S(E)$ in general are a function of temperature. Given certain reference temperature T_r, one can obtain an approximation for $\Delta\Delta F$ at any temperature T by Taylor expansion, $\Delta\Delta F(T) = \Delta\Delta F(T_r) + ((\mathrm{d}\Delta\Delta F(T))/(\mathrm{d}T))|_{T=T_r}(T - T_r) + \cdots$, which can be transformed into $\Delta\Delta F(T) = \Delta\Delta H(T_r) - T\Delta\Delta S(T_r) + \cdots$ after recalling that entropy is related to the first derivative of the free energy with respect to T, $-\Delta\Delta S = ((\mathrm{d}\Delta\Delta F)/(\mathrm{d}T))$. Thus, eq 3 can be viewed as a linear approximation for $\Delta\Delta F$ in which both entropy and enthalpy correspond to the reference temperature T_r. If the temperature dependence of $\Delta\Delta F$ is available for $T \sim T_r$, the free energy equation can be used to extract $\Delta\Delta H$ and $\Delta\Delta S$ by fitting. This is the basis of the procedure used in the protein simulation community[44] to generate entropy and enthalpy from free energy profiles obtained at multiple temperatures. In our case, the reference temperature was set to 293 K. Two more temperatures were considered, both from the replicas list, one immediately above T_r and one below it. Linear regression analysis was then run on three data points for each E and resulted in the computation of $\Delta\Delta H$ and $\Delta\Delta S$. It should be noted that in addition to the statistical error present in the sampled free energy, the entropy and enthalpy determined by fitting also contain the numerical error associated with the quality of the linear approximation. As can be seen from Figure 2, in which $\Delta\Delta H$ and $\Delta\Delta S$ are plotted, the error in the fitted functions is larger than in the free energy, but overall still small in relation to the magnitude of the functions themselves. The presence of that error should not affect our conclusions regarding the behavior of the studied properties as a function of E.

dx.doi.org/10.1021/jp509213f | J. Phys. Chem. B XXXX, XXX, XXX−XXX

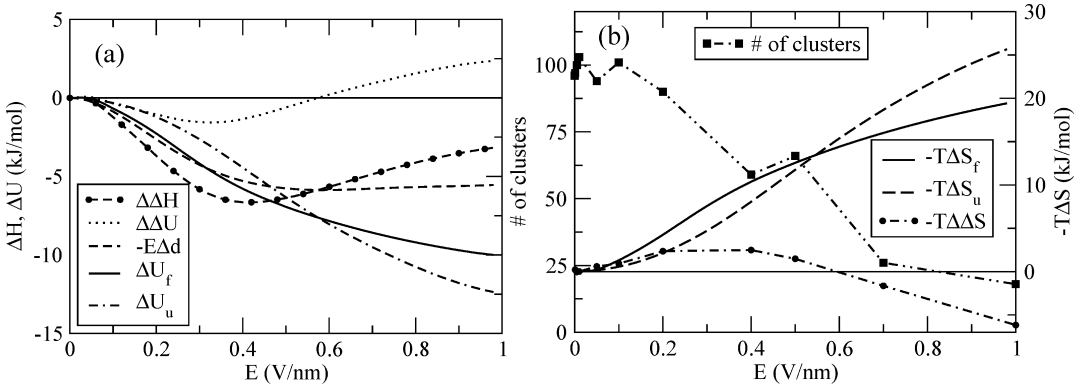

Figure 3. Electric field contributions to various thermodynamic functions discussed in the main text. Enthalpy $\Delta\Delta H$, shown in panel a, goes through a minimum at $E \sim 0.4$ V/nm, caused by specific dependence of the internal energy ΔU on the electric field in the folded and unfolded states. Entropy, shown in panel b, exhibits a maximum at the same field strength, which is due to the higher rate of decline in the entropy of the unfolded state compared to the entropy of the folded state. The latter correlates well with the decrease in the number of distinct conformational states (clusters) comprised in the unfolded state.

It can be seen in Figure 2 that the enthalpy stabilizes the native state for all E. $\Delta\Delta H$ goes through a minimum of −7 kJ/mol at $E \sim 0.4$ V/nm, after which point it rises to ∼-3 kJ/mol for the largest E considered. For $0.2 < E < 0.7$ V/nm, where the native state stabilization becomes significant, the enthalpic contribution is dominant. Entropy opposes the native state for $E < 0.6$ V/nm but begins to favor it for larger field strengths. For $E > 0.8$ V/nm, the magnitude of the entropic and enthalpic contributions to the native state stability match.

The nonmonotonic behaviors of $\Delta\Delta H$ and, especially, that of $\Delta\Delta S$ predicting that entropy stabilizes the native state, is unusual and calls for further investigation. To facilitate the analysis, the contributions due to the folded and unfolded states to these quantities were estimated separately. First, eq 1 was integrated numerically to obtain free energy components ΔF_f and ΔF_u, which were split into enthalpic, $\Delta H_{u,f}$ and entropic, $-T\Delta S_{u,f}$, contributions through fitting, using the same procedure as was done for the relative free energy $\Delta\Delta F$.

The enthalpy can be represented as a sum of two terms: $\Delta H_f = \Delta U_f - \langle d\rangle_f E$, where $\Delta U_f = U_f(E) - U_f(0)$ is the field-induced change in the internal energy of the folded state and the second term corresponds to the interaction of the permanent dipole $\langle d\rangle_f$ with the external electric field. The same decomposition can be applied for the unfolded state. The internal energy changes because the field drives the peptide into states different from those that are occupied when $E = 0$ V/nm. It should be noted, however, that the new states remain within respective folded and unfolded ensembles. With these notations, the relative enthalpy can be written as the sum of two terms: $\Delta\Delta H = \Delta\Delta U - E\Delta d$, where $\Delta\Delta U = \Delta U_f - \Delta U_u$and $\Delta d = \langle d\rangle_f - \langle d\rangle_u$. Figure 3a, in which these terms are plotted along with $\Delta\Delta H$ as a function of the electric field, shows that $\Delta\Delta H$ is dominated by the field term $-E\Delta d$ while $\Delta\Delta U$ is making only a small contribution with magnitude less than 3 kJ/mol. This observation suggests a simple mechanism for the native state stabilization at intermediate fields $0.2 < E < 0.7$ V/nm, where the enhancement of the native state is mostly enthalpic: the native state becomes more populated because it has a larger dipole moment than the unfolded state (positive Δd). This is an illustration of the intuitive expectation that the field should drive the population toward the state with the largest dipole moment. While $\Delta\Delta U$ does not make a major contribution to $\Delta\Delta H$, it is central to the appearance of the minimum in this function. Clearly, $-E\Delta d$ is a continually declining function of E that reaches a plateau at $E = 0.6$ V/nm and has no extrema. The internal energy change $\Delta\Delta U$ is a declining function for $E < 0.3$ V/nm but begins to rise for greater E. When $\Delta\Delta U$ and $-E\Delta d$ combine, the resulting function develops a minimum at $E \sim 0.4$ V/nm. Thus, the minimum in $\Delta\Delta H$ can be attributed to the minimum observed in $\Delta\Delta U$. The reason why the minimum appears can be gleaned from the comparison of the internal energy change of the folded and unfolded states,ΔU_f and ΔU_u, plotted in Figure 3a. For fields with $E < 0.55$ V/nm ΔU_f falls off faster than ΔU_u, making the difference $\Delta\Delta U$ negative. For larger field ΔU_u begins to decline faster than ΔU_f, leading to a positive $\Delta\Delta U$.

At some intermediate point $E \sim 0.3$ V/nm, $\Delta\Delta U$ goes through a minimum, as does any function that starts from zero and changes its sign from negative to positive. Thus, the specific shape of ΔU_f and ΔU_u curves is responsible for the presence of a minimum in $\Delta\Delta U$ and, as has been established, in $\Delta\Delta H$. Evidently, the minimum can be explained by the direct effect of the electric field on the conformational states of the studied system. How general this mechanism is hard to tell. The magnitude of both ΔU_f and ΔU_u depends in some nontrivial way on the geometry of the potential energy minima that correspond to the folded and unfolded state ensembles. The external field causes a redistribution of the population within these ensembles that is shaped by the depth of the minima, their width and perhaps some other parameters that may turn out to be very system specific. Whether the minimum in the relative enthalpy is shared by other proteins and, if so, whether it is caused by the minimum in $\Delta\Delta U$, remains to be seen.

The results of the entropy analysis are shown in Figure 3b. Initially, the entropy of the folded state, $-T\Delta S_f$, experiences a faster rise with E than does the entropy of the unfolded state, $-T\Delta S_u$. As a result, the transition into the native state is opposed by entropy, as indicated by positive $-T\Delta\Delta S$. For $E = 0.6$ V/nm, the contributions of the two states become equal in magnitude with $-T\Delta S_u$ overtaking $-T\Delta S_f$ for larger E, where $-T\Delta\Delta S$ becomes negative. Thus, it is clear that the reversal of the entropy role is due to its faster rate of decline with the field in the unfolded state. The key to understanding this trend is the analysis of $-T\Delta S_u$ and $-T\Delta S_f$ as a function of E.

It is convenient to analyze the influence of the electric field on the entropy in terms of the inherent structure (IS) theory,

dx.doi.org/10.1021/jp509213f | J. Phys. Chem. B XXXX, XXX, XXX−XXX

which was developed for the description of phase transitions in liquids and other disordered materials.[45] According to this theory, all conformations are unambiguously divided into basins of inherent structures that are associated with minima in the potential energy function. Jumps between ISs are interpreted as conformational changes while the movements within IS basins are treated as vibrational movements, or modes. We note that this definition of vibrational modes is much broader than the one used in classical physical chemistry, where the modes are mostly treated as harmonic. In the case of proteins, the native state can be envisioned as being comprised of one IS while the unfolded state—of many different ISs. In addition to its IS identity, each conformation possesses rotational freedom. Consequently, the influence of the electric field for the native state can be broken into two effects: (a) rotational ordering due to the alignment along the field and (b) the effect on the vibrational modes of the helical state. These two contributions are difficult to assess directly, especially the vibrational part, which depends subtly on the geometry of the potential energy minima associated with the helix.[46,47] However, an approximate estimate of the rotational effect can be obtained by computing the Shannon entropy $TS_o(E) = -kT\sum P(\Theta)\ \log(P(\Theta))$ associated with the order parameter Θ that describes the orientation of the helical conformation with respect to the field direction. Here Θ is the angle between the helix and the field axis and $P(\Theta)$ is the associated distribution function. The angle distributions were computed for native conformations (RMSD < 0.1 nm from the native state) as a function of the field strength E. In zero field the distribution is flat but acquires a narrow shape when E is increased, indicating the reduction in rotational freedom. The associated loss of entropy $TS_o(E)$ is estimated at 3.7 kJ/mol at T = 293 K when the field is varied from 0 to 1 V/nm. This constitutes less than 20% of the total entropy change in $-T\Delta S_f$, as is evident from Figure 3b. Orientational ordering thus is not the main effect in the field-driven entropy reduction of the native state at high fields. It is not negligible but does not play as an important role as does the vibrational component. Interactions with the field modify the potential energy surface of a protein (a new term is added to the Hamiltonian), directly impacting its various properties, such as $\Delta\Delta U$ or entropy. The modification is nontrivial: it can not be described, for instance, by a simple harmonic oscillator model, which does not lead to a change in the entropy of the affected system. What is observed thus is a complex nonharmonic effect that is manifested in the vibrational entropy more than in other properties.

The mechanisms of the entropy reduction discussed above also apply for the unfolded state. Additionally, the electric field may affect the number of conformations accessible in that state. To assess the effect of alignment, a number of unfolded conformations were selected and analyzed to determine the associated $TS_o(E)$ as a function of E. There was not a large variation in the obtained values, all of which were found to be close to 3.5 kJ/mol. As expected, the entropy loss is slightly lower in the unfolded state since that state has a lower dipole moment and thus should experience less prominent ordering. The field contribution to $-T\Delta\Delta S$ from the alignment effect is estimated at 0.2 kJ/mol.

To estimate the number of distinct conformational states present in the unfolded ensemble, we performed clustering of all conformations recorded in our simulations using the same parameters for all E. Note that the folded state corresponds to a single cluster in this analysis. The number of unfolded clusters N_c shown in Figure 3b drops from 100 to 20 as the field is varied between 0 and 1 V/nm. The associated entropy loss can be estimated as $T\Delta S_c = -kT\ \log(N_c(E)/N_c(0))$, which evaluates at 4 kJ/mol for the observed data and T = 293 K. Comparing this number with (a) the drop of 6 kJ/mol observed over the same range of E in the total entropy $T\Delta\Delta S$ and (b) the estimate of the contribution of rotational ordering, 0.2 kJ/mol, we conclude that the contribution of the vibrational component must be close to 2 kJ/mol. It is easy to see then that $T\Delta S_c$ accounts for more than 60% of $T\Delta\Delta S$. Thus, our analysis suggests that the ability of the electric field to eliminate unfolded conformations is the main mechanism for the entropic stabilization of the native state at E > 0.6 V/nm.

Analytical Approximation for the Effect of the Electric Field. Although $\Delta\Delta F(E)$ exhibits a rather complex and nontrivial dependence on electric field (see Figure 2) some useful analytical expressions can be obtained for it in the limit of weak E. We note that the linear dependence of the dipole moment of the folded and unfolded states (see Figure 1) allows for the following approximation to be made:

$$\langle d\rangle_f - \langle d\rangle_u = \left(\frac{\partial\langle d\rangle_f}{\partial E} - \frac{\partial\langle d\rangle_u}{\partial E}\right)E = \Delta d_0 E \tag{4}$$

When substituted into the integral of eq 2, it leads to the following quadratic approximation for the free energy:

$$\Delta\Delta F_c = -\frac{1}{2}\Delta d_0 E^2 \tag{5}$$

The empirical parameter Δd_0 can be estimated by two routes. First, we evaluated it by fitting. The numerical values of $\langle d\rangle_f$ and $\langle d\rangle_u$ recorded in the simulations were fitted by linear functions in the limit of $E \to 0$. The resulting fitting parameters led to Δd_0 = 99[kJ/mol × nm^2/V^2]. The corresponding free energy, shown in Figure 2, provides a reasonable approximation for the actual free energy for E < 0.1 V/nm.

Second, a microscopic expression was obtained for Δd_0using the cumulant expansion. Within this technique, the effect of the electric field on free energy can be represented as a series over powers of E: $F(E) = F^0 - \beta\langle d\rangle^0 E - \beta\langle d^2\rangle^0 E^2 - \cdots$, where the first term represents the free energy in the absence of the field and the other terms correspond to successive cumulant contributions. The averaging in the zero-field ensemble is indicated by $\langle\cdots\rangle^0$. The first cumulant contribution is zero because of the symmetry. The second cumulant yields the following expression, when applied to folded and unfolded states separately:

$$\Delta d_0 = \beta(\langle d^2\rangle_f^0 - \langle d^2\rangle_u^0) \tag{6}$$

The first term in the above equation can be evaluated assuming that the native state corresponds to a single conformation with the known dipole moment $\vec{P}_n$. Setting the angle between $\vec{P}_n$ and the field axis as ψ, the average over all orientations in the component parallel to $\vec{E}$ can be written as $\langle d^2\rangle_f^0 = ((\int_0^\pi P_n^2\ \cos^2(\psi)\ \sin(\psi)\ d\psi)/(\int_0^\pi \sin(\psi)\ d\psi)) = (^1/_3)\ P_n^2$, where $P_n = |\vec{P}_n|$. To obtain a similar expression for the unfolded state one needs some knowledge about its structure. Here we assume that the unfolded state is completely disordered and can be represented as a sum of N number of elementary dipole moments, for instance moments associated with the peptide bond. The total dipole then can be written as $\vec{P}_u = \sum_{i=1}^N \vec{P}_i$, where all moments $\vec{P}_i$ have the same magnitude $P = |\vec{P}|$ but different directions. Taking the average for the

dx.doi.org/10.1021/jp509213f | J. Phys. Chem. B XXXX, XXX, XXX−XXX

component parallel to the field P_u^c results in $\langle P_u^{c^2}\rangle = \langle \sum_{i,j} p_i^c p_j^c\rangle \approx N\langle p^{c^2}\rangle$, where p_i^c is the component of the ith dipole parallel to the field and the condition that the components on nonequivalent sites are uncorrelated, $\langle p_i^c p_j^c\rangle = \langle p^{c^2}\rangle \delta_{ij}$, is used. Under the assumption that elementary dipoles in unfolded conformations do not develop preferential orientations one finds that $\langle p^{c^2}\rangle = {}^1/_3\langle p^2\rangle = {}^1/_3 p^2$ and so $\langle P_u^{c^2}\rangle = N/3\ p^2$. Finally, the magnitude of the elementary moment can be related to the magnitude of the folded state as $p = (P_n/N)(1/(\cos(\phi)))$, where ϕ is the angle between each elementary dipole $\vec{p}_i$ and the total dipole of the helix $\vec{p}_n$. This relation leads to the following approximate expression for the square dipole average: $\langle d^2\rangle_u^0 = ({}^1/_3)(P_n^2/N)(1/(\cos^2(\phi)))$. When combined with the expression for the folded state, it leads to the following final result:

$$\Delta d_0^a = \beta \frac{1}{3} P_n^2 \left(1 - \frac{1}{\cos^2(\phi)} \frac{1}{N}\right) \tag{7}$$

which needs only the number of residues N and the dipole moment of the native state P_n as input. The angle ϕ is specific to the geometry of the native state. For α-helix and the parameters of OPLS/AA force-field[39] we estimated it to be 150°. The dipole moment of the folded conformations was evaluated at P_n = 31[kJ/mol x nm/V] using the ensemble average of simulations at E = 0 and N = 6. When plugged into eq 7, it produced Δd_0^a = 103[kJ/mol × nm^2/V^2], which is in excellent agreement with the value of 99[kJ/mol × nm^2/V^2] obtained directly from fitting.

How well the second cumulant approximation and the analytical expression for it work can be seen in Figure 4, which

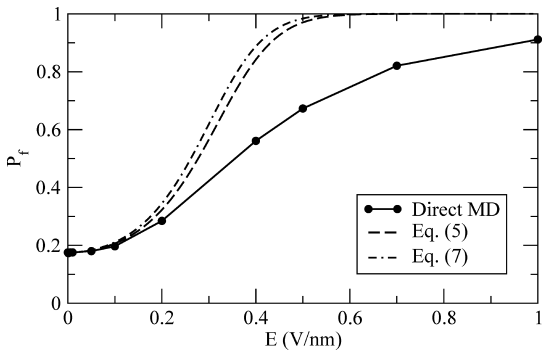

Figure 4. Population of the native state as a function of field E obtained (a) directly in simulations (b) using the quadratic approximation for free energy, eq 5, and (c) using an analytical expression for Δd_0 in the second cumulant approximation, eq 7

shows the population of the native state P_f for varying E determined (a) directly in simulation and (b) predicted from $\Delta\Delta F(E)$ by inverting eq 2. In support of the conclusion that electric field induces the coil–helix transition, P_f increases from <0.2 at E = 0 to over 0.9 at E = 1 V/nm. The approximation based on $\Delta\Delta F_c$ produces good quantitative agreement with direct simulation for E < 0.1 V/nm and overestimates P_f for other field strengths. The error is non-negligible, reaching as much as 30% for certain values of E. However, overall the second cumulant approximation provides a reasonable behavior and thus seems suitable for qualitative analysis. The analytical expression for Δd_0 generates populations in excellent agreement with the numerical results.

Three regimes can be identified in $P_f(E)$. First, for low E < 0.1 V/nm there is hardly any change in the population. This is consistent with the behavior predicted by Schwarz and Seelig[29] on the basis of the Zimm–Bragg model of the coil–helix transition. It is assumed in that model that the helix growth parameter s (free energy associated with helix elongation) can be introduced as a function of the solid angle Ω that each helical segment forms with the direction of the field. The growth parameter depends on the external field through a van't Hoff relationship.[26] The parameter increases with the field strength E, implying that helices grown along the field are more stable than those grown against it. Under the condition of no orientational polarization of the underlying conformational ensemble (all helical orientations are equally probable) the gain in population along the field is compensated for by the loss in the population against it, so that the total helix population remains unchanged. By necessity, this simple analysis contains approximations, such as the neglect of the effect of the unfolded state ensemble. Nevertheless, it predicts reasonable behavior for small E. We indeed see an enhanced helical population for conformations aligned along the field and depleted population in the conformations aligned against it. The full ensemble thus does develop orientational preference, pointing to the ordering of the native state as the main mechanism of interaction with the electric field. This is in contrast to high E, where the influence of the field on vibrational modes seems to be the main effect. Still, the ordering is not manifested in the overall population. As Figure 2 shows, the enthalpy nearly cancels the entropy in the limit of small E, leaving the free energy little changed, $\Delta\Delta F$ < 1 kJ/mol. The benefit of having conformations that gain favorable enthalpy due to the alignment with the field is lost out on the concomitant reduction in entropy. The overall effect thus is close to zero. On the basis of this analysis, we can conclude that the main effect of the field for small E is the alignment of native conformations, as has been argued previously.[25,26]

In the second regime, defined by 0.1 < E < 0.5 V/nm, the population of the native state begins to rise rapidly and suddenly. Figure 2 shows that this increase is primarily driven by enthalpy. The balance between the enthalpy and entropy observed for small E is perturbed, with the helical conformations aligned along the field making a predominant contribution to the folded state ensemble. The decrease in enthalpy can not continue indefinitely, however. At some E all helical conformations will be aligned along the field, after which point no further increase in the field strength will result in lower enthalpy. Simultaneously, the entropy of the unfolded state begins to decrease faster than the entropy of the folded state, resulting in the reversal of the entropic effect from destabilization to stabilization. The combination of these two processes leads to the emergence of saturation in $P_f(E)$ in the third regime for E > 0.5 V/nm, where the population of the native state is seen to gradually level off. We expect this qualitative behavior to be general for all disordered proteins placed in electric field.

Electric Field Causes Disaggregation of β-Sheets. To assess the effect of the electric field on aggregation we use pre-equilibrated ensemble of 8 polyalanine hexapeptides generated in replica-exchange simulations of our previous work.[38] The predominant component in that ensemble are stacked β-sheet conformations, which constitute the basic structural element of amyloid fibrils.[48] Some disordered aggregated and disaggregated states are also present. Different conformations within

dx.doi.org/10.1021/jp509213f | J. Phys. Chem. B XXXX, XXX, XXX–XXX

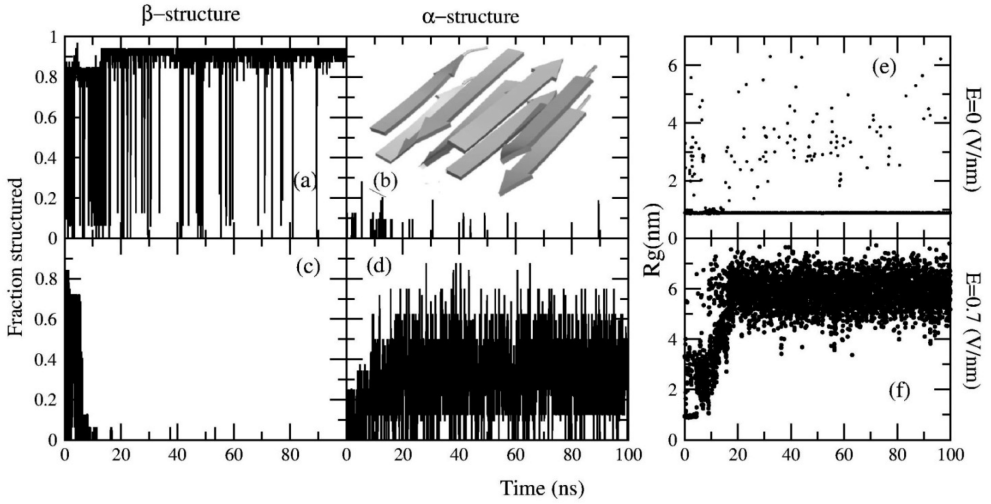

Figure 5. Time traces of various properties observed in two simulations of a pre-equilibrated ensemble of 8 polyalanine peptides. Population of β-structure is shown in panels a and c, and of α-structure, in panels b and d. Simulations in the absence of the field are shown in panels a and b, and for E = 0.7 V/nm, in panels c and d. The observed β-sheet configuration is shown in panel b. The radius of gyration for zero and nonzero field is shown in panels e and f, respectively. The application of the field causes complete loss of β-structure and conversion into α-structure, accompanied by disaggregation.

this ensemble have different permanent dipole moments. β-sheets, for instance, are expected to carry nonzero moments due to their high degree of ordering. It is not clear *a priori* how these conformations interact with the electric field and what kind of structural shifts these interactions may entail. Our simulations are conducted for 100 ns using the same parameters as reported previously[38] but in the presence of varying E. The chosen simulation time is expected to produce at least partial equilibration. All recorded conformations were preprocessed to remove ambiguities associated with the periodic boundary conditions (PBC). When processes in which two or more entities interact to form a compound are studied under PBC, their analysis requires the consideration of more than just the primary simulation cell. It may happen, for instance, that two peptides that are in the same primary cell do not make a physical contact, but their periodic images do. Therefore, all periodic images need to be analyzed in order to identify possible multipeptide complexes. Accordingly, simulated peptides and their images were clustered according to the distances among their C_α atoms. Clustering resulted in the selection of those periodic images that make interpeptide contacts. If no contacts were found, the conformations from the primary cell were considered. Clustered conformations were subjected to the secondary structure analysis due to Kabsch and Sander.[49]

The degree of aggregation in the analyzed conformations is characterized by the fraction of β-structure, P_β, which includes both β-sheet and β-bridge contributions.[49] Time traces of P_β recorded for E = 0.7 V/nm and E = 0.0 V/nm are shown in Figure 5, panels c and a, respectively. Panels b and d show the amount of α-structure (α-helix plus 3_{10}-helix[49]) measured in the same simulations. For the E = 0 case, the conformations remain 90% β-sheet (panel (a)) throughout the length of the simulation with very little α-helical structure (panel b). The majority of all conformations are compact, as is evident from the radius of gyration, shown in panel e. These results are consistent with our previous conclusions, indicating that the β-sheets remain stable over 1 μs.[38] The trace in panel c shows that the β-structure is dissolved completely within the first 10 ns when the electric field is applied. Concomitant increase in the amount of α-structure (panel d) suggests that the β-sheets are converted into α-helices. The fraction of α-structure fluctuates widely between 0 and 0.8, reflecting the fact that not all of the considered 8 peptides can be found in a helical state simultaneously. As the structural conversion progresses, the radius of gyration increases to a value of ~6*nm*, indicating that the system disaggregates. Thus, the data shown in Figure 5 for E=0.7 V/nm demonstrate that electric field disassembles β-sheets through the conformational conversion into α helices.

The microscopic reasons for the observed conversion lie in the differing dipole moments of β-sheet and α-helical phases. Figure 6 shows free energy map computed as a function of the

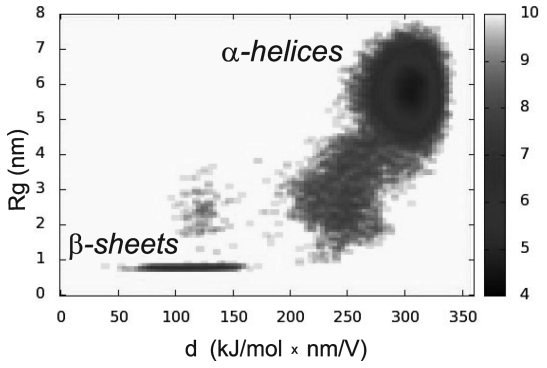

Figure 6. Free energy map defined as a function of radius of gyration R_g and the total dipole moment d, computed in the simulation with E = 0.7 V/nm. The units of energy are kT, where k is the Boltzmann constant.

radius of gyration R_g and the total dipole moment d, observed in the simulation with E = 0.7 V/nm. Computed as $-kT\log(P(d,R_g))$, where T is the temperature and $P(d,R_g)$ is the joint probability distribution function of$d$and R_g, the map reports on relative population of relevant conformational states. Two main minima are seen corresponding to the aggregated state, $R_g \sim 1nm$, which is rich in β-sheet (~90% of population) with small addition of disordered aggregates (~10% of

dx.doi.org/10.1021/jp509213f | J. Phys. Chem. B XXXX, XXX, XXX–XXX

population), and disaggregated state, $R_g > 5nm$, which is mostly α-helical. The size of individual chains observed in our simulations is broadly in agreement with that reported by Nguyen and Hall,[50] although the direct comparison is made difficult by the use of a longer alanine polypeptide by these authors. A third local minimum is seen at R_g = 3 nm and d = 250 [kJ/mol × nm/V] that corresponds to an aggregated state composed of a mixture of α-helical and random coil conformations.

The main free energy minima are well separated in the dipole moment d (Figure 6). As anticipated, the β-sheet state has a nonzero dipole with the magnitude of d = 130 [kJ/mol × nm/V]. The disaggregated state has d = 300 [kJ/mol × nm/V], which is consistent with 8 polypeptides being folded up into α-helical conformations with the dipole moment of around 37 [kJ/mol × nm/V] for each of them (see Figure 1). The difference of 170 [kJ/mol × nm/V] provides more than 100 kJ/mol of enthalpic stabilization to the disaggregated state, which is very significant. It is clear, therefore, that β-sheet conformations, as in amyloid fibrils, cannot compete with α-helical states in terms of favorable interactions with the electric field. As a result, electric fields are expected to trigger a shift toward disaggregated α-helices.

Peptides Need To Be Folded to Avoid Aggregation. The extent to which fibrils are destabilized by electric field depends on the field strength E. The average population of the β-structure $\langle P_\beta \rangle$ was computed in the multichain simulations at varying E. The result is shown in Figure 7 (broken line) as a function of the population of the native state P_f, observed for the peptide monomer under the identical thermodynamic conditions (field and temperature). As evident, the disaggregation is an all-or-none event that occurs sharply at $E \sim 0.7$ V/nm. Very little reduction is seen in the β-structure for lower E. The native state has to be approximately 90% folded in order to trigger disaggregation.

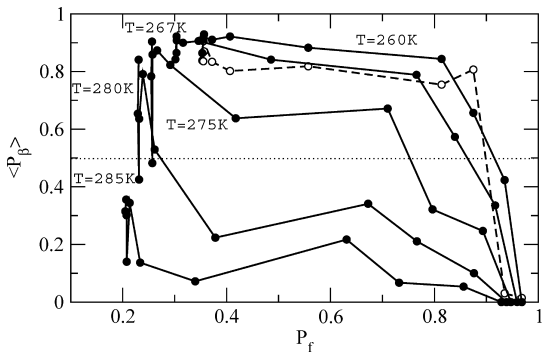

Figure 7. Average population of the β-structure $\langle P_\beta \rangle$ observed in multipeptide simulations at varying E, plotted as a function of the population of the native state P_f, obtained for the peptide monomer under identical thermodynamic conditions. Data points correspond to the values of E shown in Figure 4. Broken line represents the simulation with the box length L = 15 nm. Solid lines correspond to L = 7 nm. Data for five different temperatures are shown. Higher temperatures correspond to lower fibril stability. Disaggregation is seen when the monomer becomes folded, with P_f in the range between 0.3 and 0.9, depending on the fibril stability. In general, less stable fibrils require smaller folding enhancement to trigger disaggregation.

The details of the relationship depicted in Figure 7 undoubtedly depend on the parameters of the studied system. In particular, we tested the effect of peptide concentration and temperature. It is known that in amyloidogenic systems, low temperature and high peptide concentrations promote fibril formation.[51] The same system containing 8 peptides was considered in a smaller simulation box. While the original work used the box of length L = 15 nm,[38] an additional simulation was performed for L = 7 nm (and identical other parameters), which resulted in an approximately 10-fold increase of peptide concentration. This allowed us to obtain several other temperatures at which the fibril remains stable (on the time scale of the simulation), in addition to the lowest temperature accessible for the larger box. Figure 7 shows $\langle P_\beta \rangle$ vs P_f dependences recorded for temperature T in the range between 260 and 285 K. In the absence of the field, indicated by the very first point in every curve, it is seen that the population of the fibril drops from ~90% for T=260 K, to ~20% for T = 285 K. Therefore, the chosen range covers the fibril transition region with 280 < T < 285 K corresponding to the temperature where the fibrils melt. At the lowest studied temperature, T = 260 K, the profile of $\langle P_\beta \rangle$ recorded for L = 7 nm is very similar to that observed for L = 15 nm, indicating that concentration does not have a strong effect on aggregation propensity under conditions where the fibrils are stable. As the electric field is turned on, the population is shifted away from the fibrils. As an illustration of this tendency, at T = 275 K $\langle P_\beta \rangle$ starts at ~90% for E = 0 V/nm, corresponding to a stable fibril, and drops to ~30% at E = 0.5 V/nm, indicating that disaggregation takes place under the effect of the field. It is clear from Figure 7 that as the temperature rises, and the fibrils become less populated, it takes progressively weaker fields to completely destabilize them. While for T = 275 K, $\langle P_\beta \rangle$ drops below 50% for E = 0.5 V/nm, for T = 280 K, it does so already for E = 0.2 V/nm. In terms of the effect of the field on the native state, disaggregation is accompanied by an increase in P_f (folding enhancement) at all temperatures. This trend is consistent with numerous experimental studies on amyloidogenic proteins, which suggest that aggregation begins only after the native state is destabilized.[8,15,18] For the studied system, the field strengths required for the initiation of disaggregation give rise to P_f that varies between 0.3 and 0.9, depending on the temperature. This corresponds to the regime of rapid growth in $P_f(E)$, as seen in Figure 4. For other systems, the critical value of P_f may vary. The extent to which folding has to be enhanced in order to interfere with aggregation may need to be determined on the case-by-case basis.

Longer Peptides Experience Folding at Lower Field Intensity. The results presented in the preceding sections show that (a) electric fields are able to induce a transition into α-helical states and (b) amyloid fibrils begin to dissociate under the effect of the field if the population of the helical state is significant. However, the fields required for the transition into the native state, 0.2 < E < 0.5 V/nm, are beyond the biologically relevant scale. For reference, benchmark values for the fields encountered in biological systems are listed in Table 2. The magnitude of the listed fields increases gradually from 10^{-8} V/nm for MRI scanners to 10^{-2} V/nm estimated for the interior of cell membranes. In the high-field limit, the membrane of living cells tends to disintegrate at approximately E = 0.03 V/nm,[54] which sets the upper bound on the biologically relevant strengths. From the point of view of *in vitro* experiments, the strength of the field supported by aqueous solutions is limited by the onset of dielectric breakdown, a phenomenon taking place for the field E_b at which water transiently becomes a conductor. The exact voltages required for the breakdown

dx.doi.org/10.1021/jp509213f | J. Phys. Chem. B XXXX, XXX, XXX–XXX

Table 2. Electric Fields Relevant To Biology

system/application	electric field E (V/nm)
safe limits in MRI scanners[52]	6×10^{-9}
ground-level field requirements for high-voltage power lines[53]	1×10^{-8}
fields involved in embryonic development[54]	$(0.1-1.5) \times 10^{-7}$
bone samples[54]	2×10^{-6}
intramembrane fields[36,55]	$(1-20) \times 10^{-3}$
membrane supra-electroporation limits[54]	3×10^{-2}

depend on many factors, including the presence of cosolvents and ions, the shape of the electric pulse etc. The numbers cited in the literature for E_b vary from 0.015 V/nm[26] to anywhere between 0.01 and 0.07 V/nm with the average of about 0.03 V/nm.[56] Thus, the range of biologically relevant fields seems to agree well with the fields amenable to experimental investigations in water, which is perhaps not a coincidence.

As can be seen from Figure 4, the biologically relevant fields have no effect on the population of the native state of the model with $N = 6$. The field-induced contribution to free energy is so small for $E < 0.03$ V/nm that it leaves P_f unchanged. For the population to change appreciably, $\Delta\Delta F$ has to be comparable in magnitude to the stability of the native state ΔF. The numerical value of $\Delta\Delta F$ is defined, to a major degree, by the dipole-field contribution to the enthalpy difference $\Delta\Delta H$. Thus, one way to increase the magnitude of $\Delta\Delta F$ is to increase the magnitude of $\Delta\Delta H$. It is easy to see that $\Delta\Delta H$ scales with the dipole moment of the native state (assuming that the dipole moment of the unfolded state is negligible) for a constant field E. So, increasing the native-state dipole moment can be used as a means to increase $\Delta\Delta H$. Since the side chains in the peptide considered here carry no charge, the only source of the dipole moment is the main chain atoms. Chains with larger number of main chain atoms have larger dipole moments. The length of the peptide then can be used as a parameter to control $\Delta\Delta H$. In comparison with short chains, long chains are expected to gain more from folding up into helices (in terms of interactions with the field), hence requiring lower fields for the conversion into the helical state.

The analytical approximation for $\Delta\Delta F$ derived with the help of the cumulant expansion can be used to obtain a numerical estimate of the field required for the coil−helix transition in a peptide of arbitrary length N. Let us assume that in the absence of the field the helical conformation is characterized by free energy difference ΔF_0 with respect to the unfolded state. The stability in nonzero field then is $\Delta F(E) = \Delta F_0 + \Delta\Delta F(E) = -kT \log((P_f(E))/(1 - P_f(E)))$. Let us further assume that the population needed for disaggregation is $P_f(E_c) = P_{f,c}$, where E_c is the required critical field. A particular example is when $P_{f,c} = {}^1/_2$ that leads to the associated free energy cost $\Delta F(E_c) = \Delta F_c = 0$. Employing the quadratic approximation for $\Delta\Delta F$, eq 5, one obtains the following equation for the critical field: ${}^1/_2\Delta d_0 E_c^2 = \Delta F_0 - \Delta F_c$. Assuming that Δd_0 is given by eq 7, the solution for the field becomes $E_c = ((2(\Delta F_0 - \Delta F_c))/({}^1/_3 P_N^2(1 - (1/(\cos^2(\phi)))1/N)))^{1/2}$, where P_N is the dipole moment of the helical state. For alanine peptides, the moment can be approximated as $P_N = \alpha N$, where the proportionality constant α can be determined from $N = 6$. Under this assumption, the critical field becomes

$$E_c = \sqrt{\frac{6}{\beta\alpha^2 N^2\left(1 - \frac{1}{\cos^2(\phi)}\frac{1}{N}\right)}(\Delta F_0 - \Delta F_c)} \quad (8)$$

Figure 8 shows E_c computed using the parameters obtained for $N = 6$ for two values of the critical population $P_{f,c} = 0.3$ and

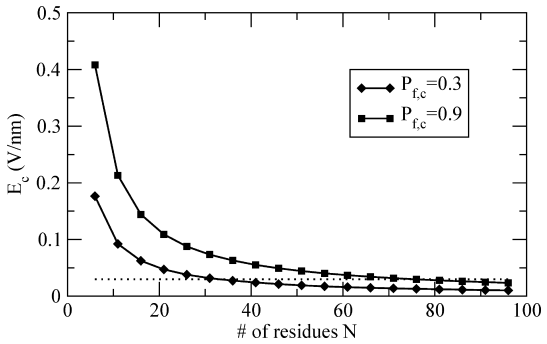

Figure 8. Critical field E_c required for the disaggregation of alanine polypeptides of length N computed using eq 8. Two values, 0.3 and 0.9, were considered for the population of the native state $P_{f,c}$. For fixed N, higher $P_{f,c}$ correspond to higher E_c. Peptides as short as 30 amino acid could be prone to disaggregation by biologically relevant fields under conditions where the fibrils are not very stable.

$P_{f,c} = 0.9$, which correspond to the range of fibril stabilities observed in our multipeptide simulations, see Figure 7. Since ΔF_0 is assumed to be constant in eq 8, but will likely decrease with N, the data shown in Figure 8 is probably an overestimation of the actual critical field. In both plotted curves, E_c rapidly decreases with the length of the chain and becomes proportional to $1/N$ in the limit of large N. The biologically relevant level of 0.03 V/nm is approached for $N \sim 30$ for the low fibril stability condition, $P_{f,c} = 0.3$, and $N \sim 70$ for the high stability limit, $P_{f,c} = 0.9$. The decreasing character of $E_c(N)$ suggests that, as their size grows, alanine-based peptides become more susceptible to the electric field. It appears that biologically relevant electric fields may prevent aggregation in peptides as short as 30 aa-long, under conditions where the fibrils are marginally stable.

To test the prediction that larger N's require smaller fields to enhance folding, we performed two additional simulations, in which the length of the peptide N was set at 14 and 50. The resulting population of the native state, shown in Figure 9,

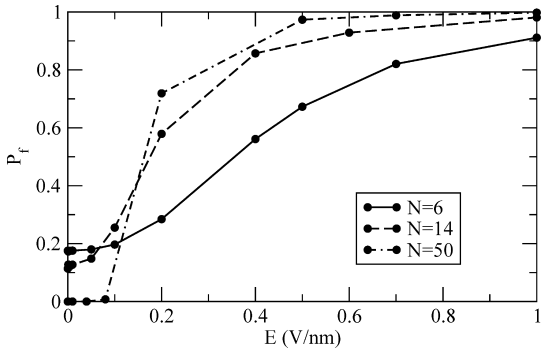

Figure 9. Population of the native helical state for alanine peptides with $N = 6$, 14, and 50 amino acid residues. Larger N is seen to require smaller E to trigger coil-to-helix transition. Lines are the guide to the eye.

dx.doi.org/10.1021/jp509213f | J. Phys. Chem. B XXXX, XXX, XXX−XXX

reveals two main effects. First, the coil−helix transition becomes sharper as N grows. Progressively, as N is increased, it takes a smaller variation in E to achieve a comparable increase in P_f. Second, the whole $P_f(E)$ curve is shifted leftward. As a consequence, longer peptides require smaller fields to achieve the same level of population, as defined, for instance, by the transition midpoint $P_f(E_m) = {}^1/_2$, as do shorter peptides. Specifically, if for $N = 6$, E_m is ∼0.4 V/nm, then for $N = 50$, it is around 0.1 V/nm. The shift is not as dramatic as suggested by our analytical calculations but still substantial and in the right direction. On the qualitative level, this result validates our conclusions regarding E_c. Indeed, for sufficiently large peptides, electric fields in the biologically relevant range may become important for both folding and aggregation.

CONCLUSIONS

Using alanine-based peptides known to form amyloid fibrils[57] as a test system we demonstrated in this paper by means of computer simulations that (a) electric field is able to induce coil−helix transition in mostly disordered systems, and (b) the resulting shift in population toward the helical state is accompanied by the dissociation of preformed β-sheets. The field thus can be used as an aggregation inhibitor. The numerical relationship between folding and aggregation determined for the test system is extrapolated to peptides of arbitrary length N. Our calculations suggest that electric fields achievable in experimental setting and relevant from biological perspective are able to alter the behavior of peptides as short as 30 aa-long, depending on the existing thermodynamic conditions. In the wider context, our results show that First, electric field may have a role in preventing aggregation in intracellular processes. The peptides associated with the Alzheimer's disease, Aβ's, are known to be cleaved from an intramembrane portion of a precursor protein.[58] It is believed that inside the membrane, the peptides form helices. The aggregation does not begin until after the peptides leave the membrane, resulting in extracellular amyloid deposition. The hydrophobic environment of the membrane interior certainly plays a role in stabilizing the helical conformations of Aβ's. But the stabilizing effect of the membrane potential can not be ruled out either. Our calculations show that electric fields due to this potential are able to alter significantly the conformational state of a disordered peptide the size of Aβ's, which is 40−43 amino acid residues depending on the variety.

Second, the electric field can be used as a tool to control aggregation of proteins in *in vitro* studies. Turning the field on or off may halt or trigger aggregation in time-resolved experiments. The advantage of this approach over other methods of imposing aggregation conducing conditions, such as addition of cosolvents, is its almost instantaneous effect. Turning the field off in solutions that are initially free of amyloid would allow one to track the progress of the aggregation reaction without experiencing any dead time. If verified experimentally, this technique could prove invaluable in the studies of early stages of aggregation, which are characterized by the formation of oligomeric species.

Third, our calculations were made for peptides that lack charged residues so that the only source of dipole moment in them is the backbone. The presence of charges on side chains may alter our conclusions significantly. It was reported, for instance, that electric field promotes the conversion of α-helices into random coils and β sheets in the Alzheimer's disease peptide Aβ1-40[59] instead of inhibiting it as predicted here. The authors were able to identify several key residues carrying electric charges that were located at the helix undergoing structural transition under the effect of the electric field. It was noted that the interactions of these residues with the applied field drove the transition to a greater extent than did the interactions of the backbone atoms. Thus, the effect of the electric field on proteins can be very specific to the primary structure and should be studied on the case-by-case basis.

Finally, we note that the reported results rely on a number of approximations. First, analytical formulas were used to compute E_c. The accuracy of these formulas remains to be tested. Second, we employed fixed-charge model for the peptide's force-field, which neglects the effect of electronic polarization due to the electric field.[60] Third, the effect of the electric field on water was neglected. Since water mediates interactions among peptide atoms, this effect may prove to be important. Fourth, the counterions that typically surround biomolecules in solution are missing in our model. The ions are known to respond to the external electric field and thus may play a role in determining folding and aggregation pathways in proteins, especially those carrying charged amino acid residues.[61]

It is easy to see that each of these approximations limits the accuracy of our predictions. Our estimate of E_c certainly contains a numerical error. Its exact magnitude, however, is difficult to estimate, given the complexity of the problem. We hope that experimental studies will be able to provide the ultimate test of the conclusions drawn in this paper. In particular, it will be very interesting to see whether amyloid fibrils made by intrinsically disordered peptides similar to those considered here can be broken up by an electric field.

AUTHOR INFORMATION

Corresponding Author

*(A.B.) E-mail: andrij@icmp.lviv.ua. Telephone: +380322761978.

Notes

The authors declare no competing financial interest.

ACKNOWLEDGMENTS

We would like to thank Wei Cai and Boris Ni for their helpful comments on the early version of the manuscript

REFERENCES

(1) Selkoe, D. J. Folding Proteins in Fatal Ways. *Nature* **2003**, *426*, 900−904.

(2) Fowler, D. M.; Koulov, A. V.; Balch, W. E.; Kelly, J. W. Functional Amyloid - from Bacteria to Humans. *Trends Biochem. Sci.* **2007**, *32*, 217−224.

(3) Otzen, D.; Nielsen, P. H. We Find Them Here, We Find Them There: Functional Bacterial Amyloid. *Cell. Mol. Life Sci.* **2008**, *65*, 910−927.

(4) Cheng, P.-N.; Liu, C.; Zhao, M.; Eisenberg, D.; Nowick, J. S. Amyloid B-Sheet Mimics That Antagonize Protein Aggregation and Reduce Amyloid Toxicity. *Nat. Chem.* **2012**, *4*, 927−933.

(5) Hard, T.; Lendel, C. Inhibition of Amyloid Formation. *J. Mol. Biol.* **2012**, *421*, 441−465.

(6) Barnham, K. J.; Kenche, V. B.; Ciccotosto, G. D.; Smith, D. P.; Tew, D. J.; Liu, X.; Perez, K.; Cranston, G. A.; Johanssen, T. J.; Volitakis, I.; et al. Platinum-Based Inhibitors of Amyloid-Beta as Therapeutic Agents for Alzheimer's Disease. *Proc. Natl. Acad. Sci. U.S.A.* **2008**, *105*, 6813−6818.

(7) Rajagopal, K.; Schneider, J. P. Self-Assembling Peptides and Proteins for Nanotechnological Applications. *Curr. Opin. Struct. Biol.* **2004**, *14*, 480−486.

(8) Dobson, C. M. Protein Folding and Misfolding. *Nature* **2003**, *426*, 884−890.
(9) Ramirez-Alvarado, M.; Merkel, J. S.; Regan, L. A Systematic Exploration of the Influence of the Protein Stability on Amyloid Fibril Formation in Vitro. *Proc. Natl. Acad. Sci. U.S.A.* **2000**, *97*, 8979−8984.
(10) Munishkina, L. A.; Henriques, J.; Uversky, V. N.; Fink, A. L. Role of Protein-Water Interactions and Electrostatics in Alpha-Synuclein Fibril Formation. *Biochemistry* **2004**, *43*, 3289−3300.
(11) Brockwell, D. J.; Radford, S. E. Intermediates: Ubiquitous Species on Folding Energy Landscapes? *Curr. Opin. Struct. Biol.* **2007**, *17*, 30−37.
(12) Jahn, T. R.; Radford, S. E. Folding Versus Aggregation: Polypeptide Conformations on Competing Pathways. *Arch. Biochem. Biophys.* **2008**, *469*, 100−117.
(13) Hurle, M. R.; Helms, L. R.; Li, L.; Chan, W. N.; Wetzel, R. A Role for Destabilizing Amino-Acid Replacements in Light-Chain Amyloidosis. *Proc. Natl. Acad. Sci. U.S.A.* **1994**, *91*, 5446−5450.
(14) Lai, Z. H.; Colon, W.; Kelly, J. W. The Acid-Mediated Denaturation Pathway of Transthyretin Yields a Conformational Intermediate That Can Self-Assemble into Amyloid. *Biochemistry* **1996**, *35*, 6470−6482.
(15) Booth, D. R.; Sunde, M.; Bellotti, V.; Robinson, C. V.; Hutchinson, W. L.; Fraser, P. E.; Hawkins, P. N.; Dobson, C. M.; Radford, S. E.; Blake, C. C. F.; et al. Instability, Unfolding and Aggregation of Human Lysozyme Variants Underlying Amyloid Fibrillogenesis. *Nature* **1997**, *385*, 787−793.
(16) Kelly, J. W. The Alternative Conformations of Amyloidogenic Proteins and Their Multi-Step Assembly Pathways. *Curr. Opin. Struct. Biol.* **1998**, *8*, 101−106.
(17) Chiti, F.; Taddei, N.; Bucciantini, M.; White, P.; Ramponi, G.; Dobson, C. M. Mutational Analysis of the Propensity for Amyloid Formation by a Globular Protein. *EMBO J.* **2000**, *19*, 1441−1449.
(18) Uversky, V. N.; Fink, A. L. Conformational Constraints for Amyloid Fibrillation: The Importance of Being Unfolded. *Biochim. Biophys. Acta* **2004**, *1698*, 131−153.
(19) Chiti, F.; Taddei, N.; Baroni, F.; Capanni, C.; Stefani, M.; Ramponi, G.; Dobson, C. M. Kinetic Partitioning of Protein Folding and Aggregation. *Nat. Struct. Biol.* **2002**, *9*, 137−143.
(20) Chiti, F.; Taddei, N.; Stefani, M.; Dobson, C. M.; Ramponi, G. Reduction of the Amyloidogenicity of a Protein by Specific Binding of Ligands to the Native Conformation. *Protein Sci.* **2001**, *10*, 879−886.
(21) Nerelius, C.; Sandegren, A.; Sargsyan, H.; Raunak, R.; Leijonmarck, H.; Chatterjee, U.; Fisahn, A.; Imarisio, S.; Lomas, D. A.; Crowther, D. C.; et al. Alpha-Helix Targeting Reduces Amyloid-Beta Peptide Toxicity. *Proc. Natl. Acad. Sci. U.S.A.* **2009**, *106*, 9191−9196.
(22) Villegas, V.; Zurdo, J.; Filimonov, V. V.; Aviles, F. X.; Dobson, C. M.; Serrano, L. Protein Engineering as a Strategy to Avoid Formation of Amyloid Fibrils. *Protein Sci.* **2000**, *9*, 1700−1708.
(23) Abedini, A.; Raleigh, D. P. A Critical Assessment of the Role of Helical Intermediates in Amyloid Formation by Natively Unfolded Proteins and Polypeptides. *Protein Eng., Des. Sel.* **2009**, *22*, 453−459.
(24) Porschke, D. Effects of Electric-Fields on Bio-Polymers. *Annu. Rev. Phys. Chem.* **1985**, *36*, 159−178.
(25) Porschke, D. Macrodipoles - Unusual Electric Properties of Biological Macromolecules. *Biophys. Chem.* **1997**, *66*, 241−257.
(26) Neumann, E. Chemical Electric-Field Effects in Biological Macromolecules. *Prog. Biophys. Mol. Biol.* **1986**, *47*, 197−231.
(27) Diekmann, S.; Hillen, W.; Jung, M.; Wells, R. D.; Porschke, D. Electric Properties and Structure of DNA Restriction Fragments from Measurements of the Electric Dichroism. *Biophys. Chem.* **1982**, *15*, 157−167.
(28) Porschke, D. Electric, Optical and Hydrodynamic Parameters of Lac Repressor from Measurements of the Electric Dichroism - High Permanent Dipole-Moment Associated with the Protein. *Biophys. Chem.* **1987**, *28*, 137−147.
(29) Schwarz, G.; Seelig, J. Kinetic Properties and the Electric Field Effect of Life Helix-Coil Transition of Poly(Gamma-Benzyl L-Glutamate) Determined from Dielectric Relaxation Measurements. *Biopolymers* **1968**, *6*, 1263−1277.
(30) Schwarz, G. On Kinetics of Helix-Coil Transition of Polypeptides in Solution. *J. Mol. Biol.* **1965**, *11*, 64.
(31) Wada, A. Dielectric Evidence of Chemical Relaxation in the Helix-Coil Transition of Polypeptides. *Chem. Phys. Lett.* **1971**, *8*, 211−213.
(32) Marchal, E. Comment on Wadas Letter on Dielectric Evidence of Chemical Relaxation in Helix-Coil Transition of Polypeptides. *Chem. Phys. Lett.* **1971**, *12*, 9.
(33) Sano, T.; Yasunaga, T. Kinetics of Helix-Coil Transition of Polypeptides in Solution by the Relaxation Methods. *Biophys. Chem.* **1980**, *11*, 377−386.
(34) Porschke, D. Electrostatics and Electrodynamics of Bacteriorhodopsin. *Biophys. J.* **1996**, *71*, 3381−3391.
(35) Rochu, D.; Pernet, T.; Renault, F.; Bon, C.; Masson, P. Dual Effect of High Electric Field in Capillary Electrophoresis Study of the Conformational Stability of Bungarus Fasciatus Acetylcholinesterase. *J. Chromatogr. A* **2001**, *910*, 347−357.
(36) Astumian, D.; Berg, H. Direct Electric-Field Effects and Sequential Processes in Biosystems. *Bioelectrochem. Bioenerg.* **1991**, *25*, 455−462.
(37) Shoemaker, K. R.; Kim, P. S.; York, E. J.; Stewart, J. M.; Baldwin, R. L. Tests of the Helix Dipole Model for Stabilization of Alpha-Helices. *Nature* **1987**, *326*, 563−567.
(38) Ni, B.; Baumketner, A. Reduced Atomic Pair-Interaction Design (Rapid) Model for Simulations of Proteins. *J. Chem. Phys.* **2012**, *138*, 064102.
(39) Kaminski, G. A.; Friesner, R. A.; Tirado-Rives, J.; Jorgensen, W. L. Evaluation and Reparametrization of the Opls-Aa Force Field for Proteins Via Comparison with Accurate Quantum Chemical Calculations on Peptides. *J. Phys. Chem. B* **2001**, *105*, 6474−6487.
(40) Sugita, Y.; Okamoto, Y. Replica-Exchange Molecular Dynamics Method for Protein Folding. *Chem. Phys. Lett.* **1999**, *314*, 141−151.
(41) Van der Spoel, D.; Lindahl, E.; Hess, B.; Groenhof, G.; Mark, A. E.; Berendsen, H. J. C. Gromacs: Fast, Flexible, and Free. *J. Comput. Chem.* **2005**, *26*, 1701−1718.
(42) Hess, B.; Kutzner, C.; van der Spoel, D.; Lindahl, E. Gromacs 4: Algorithms for Highly Efficient, Load-Balanced, and Scalable Molecular Simulation. *J. Chem. Theory Comput.* **2008**, *4*, 435−447.
(43) Allen, M. P.; Tildesley, D. J. *Computer Simulations of Liquids*; Oxford University Press: Oxford, U.K., 1987.
(44) Garcia, A. E.; Onuchic, J. N. Folding a Protein in a Computer: An Atomic Description of the Folding/Unfolding of Protein A. *Proc. Natl. Acad. Sci. U.S.A.* **2003**, *100*, 13898−903.
(45) Stillinger, F. H.; Weber, T. A. Hidden Structure in Liquids. *Phys. Rev. A* **1982**, *25*, 978−989.
(46) Baumketner, A.; Shea, J. E.; Hiwatari, Y. Glass Transition in an Off-Lattice Protein Model Studied by Molecular Dynamics Simulations. *Phys. Rev. E* **2003**, *67*, 011912.
(47) Friedel, M.; Baumketner, A.; Shea, J. E. Stability of a Protein Tethered to a Surface. *J. Chem. Phys.* **2007**, *126*.
(48) Serpell, L. C.; Fraser, P. E.; Sunde, M. X-Ray Fiber Diffraction of Amyloid Fibrils. In *Methods in Enzymology*; Ronald, W., Ed.; Academic Press: San Diego, CA, 1999; Vol. *309*, pp 526−536.
(49) Kabsch, W.; Sander, C. Dictionary of Protein Secondary Structure - Pattern-Recognition of Hydrogen-Bonded and Geometrical Features. *Biopolymers* **1983**, *22*, 2577−2637.
(50) Nguyen, H. D.; Hall, C. K. Phase Diagrams Describing Fibrillization by Polyalanine Peptides. *Biophys. J.* **2004**, *87*, 4122−4134.
(51) Harper, J. D.; Wong, S. S.; Lieber, C. M.; Lansbury, P. T. Observation of Metastable A? Amyloid Protofibrils by Atomic Force. *Chem. Biol.* **1997**, *4*, 119−125.
(52) Schlueter, R. D.; Budinger, T. F. Magic Angle Rotating. Field Nmr/Mri Magnet for in Vivo Monitoring of Tissue. *IEEE Trans. Appl. Supercond.* **2008**, *18*, 864−867.
(53) Wiggins, C. M.; Wright, S. E. Switching Transient Fields in Substations. *IEEE Trans. Power Delivery* **1991**, *6*, 591−600.

(54) Sheppard, A. R.; Swicord, M. L.; Balzano, Q. Quantitative Evaluations of Mechanisms of Radiofrequency Interactions with Biological Molecules and Processes. *Health Phys.* **2008**, *95*, 365−396.
(55) Astumian, R. D.; Robertson, B. Nonlinear Effect of an Oscillating Electric-Field on Membrane-Proteins. *J. Chem. Phys.* **1989**, *91*, 4891−4901.
(56) Stygar, W. A.; Wagoner, T. C.; Ives, H. C.; Wallace, Z. R.; Anaya, V.; Corley, J. P.; Cuneo, M. E.; Harjes, H. C.; Lott, J. A.; Mowrer, G. R.; et al. Water-Dielectric-Breakdown Relation for the Design of Large-Area Multimegavolt Pulsed-Power Systems. *Phys. Rev. Spec. Top.—Accel. Beams* **2006**, *9*, 070401.
(57) Blondelle, S. E.; Forood, B.; Houghten, R. A.; PerezPaya, E. Polyalanine-Based Peptides as Models for Self-Associated Beta-Pleated-Sheet Complexes. *Biochemistry* **1997**, *36*, 8393−8400.
(58) Rochet, J.-C.; Lansbury, P. T., Jr. Amyloid Fibrillogenesis: Themes and Variations. *Curr. Opin. Struct. Biol.* **2000**, *10*, 60−68.
(59) Toschi, F.; Lugli, F.; Biscarini, F.; Zerbetto, F. Effects of Electric Field Stress on a Beta-Amyloid Peptide. *J. Phys. Chem. B* **2009**, *113*, 369−376.
(60) Calvo, F.; Dugourd, P. Folding of Gas-Phase Polyalanines in a Static Electric Field: Alignment, Deformations, and Polarization Effects. *Biophys. J.* **2008**, *95*, 18−32.
(61) Yoshioka, K.; Fujimori, M.; Kikuchi, K. Electro-Optical Studies on the Electric Field-Induced Helix-to-Coil Transition of Poly(L-Ornithine Hydrobromide) in Methanol-Water Mixtures. *Int. J. Biol. Macromol.* **1980**, *2*, 213−216.